Check for updates

Paleoceanography and Paleoclimatology

RESEARCH ARTICLE
10.1029/2021PA004283

Key Points:

- Last Millennium data assimilation products show intensification of Eastern Pacific (EP) El Niño events in the 20th century, but no change in Central Pacific (CP) frequency
- Shifts in El Niño hydroclimate teleconnections over North America are variable in magnitude, but consistent in sign over the Last Millennium
- Inconsistent results between CP and EP El Niño definitions suggest a need for more robust, spatially dependent classification schemes

Supporting Information:

Supporting Information may be found in the online version of this article.

Correspondence to:

X. Luo,
xl91@rice.edu

Citation:

Luo, X., Dee, S., Stevenson, S., Okumura, Y., Steiger, N., & Parsons, L. (2022). Last Millennium ENSO diversity and North American teleconnections: New insights from paleoclimate Data Assimilation. *Paleoceanography and Paleoclimatology*, *37*, e2021PA004283. https://doi.org/10.1029/2021PA004283

Received 14 APR 2021
Accepted 7 FEB 2022

© 2022. American Geophysical Union. All Rights Reserved.

Last Millennium ENSO Diversity and North American Teleconnections: New Insights From Paleoclimate Data Assimilation

Xinyue Luo[1], Sylvia Dee[1], Samantha Stevenson[2], Yuko Okumura[3], Nathan Steiger[4,5], and Luke Parsons[6]

[1]Department of Earth, Environmental, and Planetary Sciences, Rice University, Houston, TX, USA, [2]Bren School of Environmental Science and Management, University of California, Santa Barbara, CA, USA, [3]Institute for Geophysics, Jackson School of Geosciences, University of Texas at Austin, Austin, TX, USA, [4]Institute of Earth Sciences, Hebrew University of Jerusalem, Jerusalem, Israel, [5]Lamont-Doherty Earth Observatory, Columbia University, Palisades, NY, USA, [6]Nicholas School of the Environment, Duke University, Durham, NC, USA

Abstract El Niño-Southern Oscillation (ENSO) variability affects year-to-year changes in North American hydroclimate. Extra-tropical teleconnections are not always consistent between El Niño events due to stochastic atmospheric variability and diverse sea surface temperature anomalies, making it difficult to quantify teleconnections using only instrumentally-based records. Here we use two paleoclimate data assimilation (DA) products spanning the Last Millennium (LM) to compare changes in amplitudes and frequencies of diverse El Niño events during the pre-industrial period and 20th century, and to assess the stationarity of their North American hydroclimate impacts on multi-decadal to centennial timescales. Using several definitions for Central Pacific (CP) and Eastern Pacific (EP) El Niño, we find a marked increase in 20th century EP El Niño intensity, but no significant changes in CP or EP El Niño frequencies in response to anthropogenic forcing. The associated hydroclimate anomalies indicate (a) dry conditions across the eastern-central and northwestern U.S. during CP El Niño and wetter conditions in the same regions during EP El Niño; (b) wet conditions over the southwestern U.S. for both El Niño types. The magnitude of regional hydroclimate teleconnections also shows large natural variability on multi-decadal to centennial timescales. However, when the entire LM is considered, mean hydroclimate anomalies in North America during CP or EP El Niño are consistent in terms of sign (wet vs. dry). Results are sensitive to proxy data and model priors used in DA products. Inconsistencies between El Niño classification methods underscore the need for improved ENSO diversity classification when assessing precipitation teleconnections.

1. Introduction

The El Niño-Southern Oscillation (ENSO) dominates interannual climate variability in the tropical Pacific (Trenberth, 1997). Large variations in sea surface temperature (SST) associated with ENSO can induce large shifts in atmospheric circulation; these shifts in turn affect hydroclimate in the midlatitudes, including North America. For example, ENSO exacerbates extreme events in the United States such as California drought (Griffin & Anchukaitis, 2014; Seager & Hoerling, 2014) and flooding on the Mississippi (Munoz & Dee, 2017). Improving our understanding of the interactions between extreme hydroclimate events and variability in ENSO's North American teleconnections is therefore of paramount importance.

While ENSO is associated with SST warming/cooling anomalies in the equatorial Pacific, the patterns of SST anomalies may vary; generally El Niño and La Niña events are classified into events having centers of action in the eastern Pacific (EP) or central Pacific (CP), which have distinct hydroclimate signatures (Capotondi et al., 2015). Many studies have labeled these ENSO "flavors" (Trenberth & Stepaniak, 2001) (e.g., CP vs. EP ENSO) to track and partition ENSO teleconnection impacts (Larkin & Harrison, 2005b; Ashok et al., 2007; Kao & Yu, 2009; Yeh et al., 2009; Weng et al., 2007, 2009). However, there is still substantial debate surrounding whether or not the different flavors of ENSO represent two distinct modes, or are simply part of a continuum of SST patterns (Giese & Ray, 2011; Johnson, 2013; Okumura, 2019; Timmermann et al., 2018; Williams & Patricola, 2018). ENSO diversity inherently complicates our understanding of ENSO teleconnections, because changes in SST patterns during ENSO have been shown to have distinct impacts on precipitation in North America (Johnson & Kosaka, 2016; Patricola et al., 2020; Shin et al., 2010; Weng et al., 2007, 2009). Some work has assumed that

ENSO-induced teleconnections are quasi-stationary (Diaz et al., 2001; Sterl et al., 2007), implying that similar extratropical changes in surface temperature and precipitation could be expected given two events with similar amplitudes and distributions of sea surface temperature anomalies (SSTAs) (Ting & Hoerling, 1993). However, observations show that teleconnections differ widely between individual ENSO events (Changnon, 1999; Hoell et al., 2016; Hoerling & Kumar, 1997; Larkin & Harrison, 2005a; Paek et al., 2017; Siler et al., 2017). Internal atmospheric variability contributes to distinct responses to SST patterns, which modulate ENSO teleconnection expression (Deser et al., 2017; Hoell et al., 2016; Lloyd et al., 2009, 2011, 2012; Stevenson et al., 2015). Finally, there are low-frequency modulations in average teleconnection precipitation patterns evident over decadal-to-centennial timescales (Ashcroft et al., 2016; Coats et al., 2013; Lewis & LeGrande, 2015).

Given the strong internal variability in both ENSO-related SST and hydroclimate teleconnections, current observational data is too short (~100 years) to sufficiently characterize the complexity of ENSO diversity and its teleconnections (Stevenson et al., 2012). A longer, continuous, and high-resolution observational baseline is needed to elucidate our understanding of ENSO impacts on North American hydroclimate. To this end, highly resolved paleoclimate archives and new techniques in paleoclimate data assimilation can be used to augment instrumental data and constrain the behavior of ENSO flavors and their teleconnections. The Last Millennium (LM) is an ideal period for studying ENSO teleconnection characteristics because of the existence of numerous paleoclimate records and the dominance of multi-decadal variability prior to the onset of anthropogenic greenhouse forcing. SST reconstructions based on ocean sediments and coral records show that ENSO activity varied during different periods of the LM (Cobb et al., 2003; Rustic et al., 2015) in terms of frequency and amplitude of CP and EP El Niño events (Freund et al., 2019; Liu et al., 2017). For example, coral and tree ring reconstructions suggest an increasing frequency of CP El Niño events in the late of 20th century, attributable to changes in the mean state of SST under anthropogenic warming (Freund et al., 2019; Liu et al., 2017).

Despite the relatively rich data availability over the LM, to date, few studies have focused on the impact of ENSO diversity on hydroclimate anomalies in North America. Indeed, given the limited spatiotemporal coverage in the paleoclimate record, it is difficult to analyze the full spatial imprint of the ENSO system on a continuous time series, and with the spatial resolution necessary to capture SST pattern diversity. Thus, in this study, we use two paleoclimate data assimilation (DA) reconstructions spanning the LM. The combination of annually resolved, multi-proxy paleoclimate data and coupled climate model output facilitates DA reconstruction of past climate information derived jointly from paleo-archives and model physics with complete spatial resolution. The two paleoclimate DA reconstructions employed include the Last Millennium Reanalysis (LMR, Hakim et al. (2016); Tardif et al. (2019)) and the Paleo Hydrodynamics Data Assimilation product (PHYDA, Steiger et al. (2018)), both of which are used to investigate ENSO's behavior over the LM. The two products allow us to identify ENSO events and SST anomaly patterns, and to assess the associated hydroclimate anomalies across North America in a physically consistent framework.

This study focuses on changes in the frequency and hydroclimate expression of CP and EP El Niño events between the pre-industrial period (1000–1850 C.E.) and the 20th century (1900–2000 C.E.). Given that multiple studies demonstrate that CP and EP La Niña events are not easy to partition (Kug & Ham, 2011; Ren & Jin, 2011; Zhang et al., 2015), and the fact that many of the methods described in this study focus solely on El Niño events, we opt to examine CP and EP El Niño events alone. We investigate the impacts of CP and EP El Niño on the hydroclimate over North America in both data products, with specific attention to three key questions: (a) Are teleconnections during CP and EP El Niño events self-consistent across different definitions classifying CP and EP El Niño? (b) Are the teleconnections associated with EP and CP El Niño events themselves changing with time? (c) What do changes to the frequency and/or intensity of CP and EP El Niño with time imply about future changes in North American hydroclimate for different SSTA patterns?

2. Data and Methods

2.1. Data Assimilation Reconstructions

The data assimilation reconstructions used in this study are the Last Millennium Reanalysis (LMR, Hakim et al. (2016); Tardif et al. (2019)) and the Paleo Hydrodynamics Data Assimilation Product (PHYDA, Steiger et al. (2018)). Both DA products blend paleoclimate proxy data with global climate model simulations in an offline ensemble Kalman filter approach (Oke et al., 2002). Constrained by both observations and our knowledge

of climate dynamics, these data assimilation-based reconstructions produce annually resolved and spatially continuous data of climate history over the last 2000 years.

2.1.1. The Last Millennium Reanalysis (LMR)

LMR (Hakim et al., 2016; Tardif et al., 2019) reconstructs several annually resolved climate variables, including SST and the Palmer Drought Severity Index (PDSI, Palmer (1965)), as used here. The annual anomalies are reconstructed based on calendar year averaging (e.g., Jan.1997–Dec.1997), which splits years in the middle of peak ENSO cycles (December-February, DJF). Two versions of the LMR have been developed; we employ LMR versions 2.0 (v2.0) and 2.1 (v2.1), which include an updated proxy database and seasonal regression-based models for tree-ring width. By contrast, LMR version 1 used annual regression-based models for all proxies (Tardif et al., 2019). LMR v2.0 uses a database of 2,244 proxies (Anderson et al., 2019) that combines PAGES2k records (PAGES2k Consortium, 2017) and Breitenmoser et al. (2014) chronologies, whereas LMR v2.1 uses only 544 records from PAGES2k Consortium (2017) spanning varying portions of the Common Era. LMR generally assimilates temperature-sensitive proxies. Proxies are modeled as univariate with respect to annual temperature, except in the case of tree ring width, which is bivariate with respect to seasonal temperature and precipitation. Additionally, LMR employs the Last Millennium simulation from the Community Climate System Model version 4 (CCSM4, Landrum et al. (2013)) as its prior, from which 100 years were randomly drawn in the data assimilation process. The LMR reconstructions also include a suite of Monte-Carlo iterations, each of which withholds 25% of randomly selected proxies in the reconstruction process and includes a different random draw of 100 years from CCSM4. Here we employ the ensemble mean SST and PDSI of all ensemble members and Monte-Carlo iterations to investigate ENSO diversity and hydroclimate teleconnection patterns.

To investigate the sensitivity of our results to the proxy network used for the reconstruction, we analyzed data from two additional LMR experiments that changed the proxy availability or regional coverage used in the reconstruction (Section 3.2). The first experiment employs a fixed-proxy reconstruction (e.g., a fixed number of proxies are used throughout the LM in the assimilation). This effectively accounts for the impacts of variance reduction back in time caused by the reduction of proxy availability used in the original LMR reconstructions (Figure S1 in the Supporting Information S1). This allows for the comparison of temporal variance changes without proxy network changes. A second experiment reconstructs climate withholding all North American proxy records to mask the regional proxy impacts on SST reconstructions. This experiment investigates the impact of regional proxy availability (used in L. Parsons and Hakim (2019)) on our results of CP and EP El Niño characteristics.

2.1.2. The Paleo Hydrodynamics Data Assimilation Product (PHYDA)

PHYDA (Steiger et al., 2018) combines 2978 proxy time series with a climatologically bias-corrected version of one full-forcing Community Earth System Model Last Millennium Ensemble member (CESM LME, Otto-Bliesner et al. (2016)). In contrast to the LMR, PHYDA is specifically designed around a hydroclimate-sensitive proxy network. The proxies used in PHYDA are modeled as univariate with either temperature or PDSI, or as bivariate with SST and sea surface salinity. PHYDA reconstructs climate variables at resolutions of annual mean, boreal summer mean (June through August; JJA), and austral summer mean (December through February; DJF); of these we use 2m air temperature and PDSI at annual mean resolution. Unlike LMR, PHYDA's annual mean is based on a hydrological year (April to March of next year, e.g., Apr.1997-Mar.1998), better preserving peak ENSO impacts. Similar to the LMR, we use the ensemble mean of PHYDA for our analyses (PHYDA's ensemble is derived from all the years from the bias-corrected CESM LME simulation). Two-meter (2m) air temperature is used as an approximation for tropical Pacific SST in PHYDA (SST is not directly reconstructed, though over the open ocean 2m air temperature is very highly correlated with SST (Cayan, 1980)).

2.2. Definitions

We employ multiple definitions to characterize El Niño events, El Niño spatial pattern differences, and associated hydroclimate teleconnections. Given the joint impacts of changes in climate mean state and reconstruction variance back in time, all variable anomalies are computed following the removal of the running 30-year mean, and standard deviations are computed using a 30-year moving window.

2.2.1. ENSO Event Classification

In this paper, El Niño/La Niña events are defined with Niño 3.4 index in both DA products. Note that La Niña events are considered only for the validation of the two DA products; the focus of our analysis is El Niño events only. The 30-year running mean is removed to calculate SSTA; the Niño 3.4 index is computed using SSTA averaged over the Niño 3.4 region (5°S-5°N, 170-120°W). An El Niño event is classified for Niño 3.4 index anomalies exceeding +1 standard deviation (+1σ). Conversely, a La Niña event falls below -1σ.

2.2.2. Central Pacific and Eastern Pacific El Niño Events

Central Pacific (CP) (also called Modoki (Ashok et al., 2007)) and Eastern Pacific (EP) El Niño events refer to the spatial differences in SSTA maxima and SSTA patterns observed over the modern period (Kao & Yu, 2009). Several indices and methods have been employed in the literature to differentiate between CP and EP El Niño, and to better understand El Niño diversity. Noting the complexity in SSTA patterns, some El Niño events occur over a broad range of longitudes covering both CP and EP. The identification of CP and EP El Niño is thus not strictly binary, and depends on the methodology employed (Capotondi et al., 2015). With attention to the impact of the methodology, we here summarize three such index definitions:

2.2.2.1. Niño 3–4 Index

The Niño 3–4 index method (Kug et al., 2009; Yeh et al., 2009) classifies El Niño events as "warm pool" or "cold tongue." "Warm pool" events, which are treated as CP El Niño in this paper, are defined as years when average SSTA in Niño 4 region (5°S-5°N, 160°E−150°W) (a) exceeds 1σ, and (b) exceeds the average SSTA in the Niño 3 region (5°S-5°N, 150-90°W). "Cold tongue" events (EP El Niño) are conversely characterized when Niño 3 region SSTA exceeds 1σ and average Niño 4 SSTA.

2.2.2.2. CP-EP Index

The CP-EP index method (Kao & Yu, 2009; Yu et al., 2012) uses regression and Empirical Orthogonal Function (EOF) analysis. To obtain the CP El Niño structure, the regression of the Niño 1 + 2 index (SSTA averaged over 0°-10°N, 90°-80°W) onto SSTA is subtracted from original tropical SSTA field before EOF analysis is applied to the SSTA over the tropical Pacific (30°S-30°N, 120°E−80°W). The leading principal component (PC) of this EOF analysis is used to define the CP index. For EP El Niño, a similar removal of the Niño 4 regression onto SSTA is conducted and EOF analysis on tropical Pacific SSTA is used to obtain the leading PC as the EP index. CP El Niño is characterized as CP index years above 1σ, where the CP index also exceeds the EP index, and vice versa for EP El Niño.

2.2.2.3. C and E Index

The C and E index method (Takahashi et al., 2011) defines "C" and "E" indices to represent CP and EP El Niño events, respectively. These indices are defined by a linear combination of the first two PCs of tropical Pacific SSTA, effectively forming a 45°-rotated orthogonal coordinate:

$$C = (PC1 + PC2)/\sqrt{2},$$

$$E = (PC1 - PC2)/\sqrt{2}.$$

CP El Niño is then defined as C index years exceeding 1σ and C index exceeding E index, and vice versa for EP El Niño.

2.2.3. Hydroclimate Teleconnections and SST Composites

We use PDSI to evaluate changes in North American hydroclimate conditions (positive PDSI represents wet conditions, and negative PDSI represents dry conditions). PHYDA does not reconstruct precipitation amount directly, but PDSI is a reconstructed state variable in both DA reconstructions. Thus, we used PDSI to facilitate consistent comparisons between LMR and PHYDA. In our analysis, PDSI is normalized by the 30-year running standard deviation of the Niño 3.4 index to isolate El Niño teleconnection hydroclimate signals from changes in mean state climate (Stevenson, 2012; S. Dee et al., 2020). We computed patterns of El Niño and hydroclimate teleconnections through creating composites of SSTA and normalized PDSI anomalies (Stevenson et al., 2012). For the comparison between the pre-industrial period and the 20th century, we computed the probability density

functions (PDFs) of variables of interest (e.g., event indices and normalized PDSI) during the two time periods to investigate climatic shifts.

3. Results

3.1. Validation of ENSO Characteristics in Paleo-DA Reconstructions

Biases in the reconstructions employed here exist due to uncertainties in proxies and reconstruction methodology (Hakim et al., 2016; Steiger et al., 2018; Tardif et al., 2019). Thus, to validate ENSO characteristics in the LMR and PHYDA ((Figures S2 and S3 in the Supporting Information S1), we compare both datasets to 20th century (1900–2000) observations of SST from the Hadley Center (HadISST v1.1, Rayner et al. (2003)). Comparisons show that, in general, El Niño events (defined according to Niño 3.4 index, Section 2.2.1) derived from LMR v2.1 and PHYDA show strong similarities with observations in terms of both SSTA patterns and the statistics of Niño 3.4 index variability (Figures S2 and S3 in the Supporting Information S1).

The El Niño SSTA pattern in LMR v2.1 differs from observations near the eastern tropical Pacific coast (Figure S2c in the Supporting Information S1), likely reflecting known biases in CCSM4: the ENSO SSTA patterns are shifted west relative to observations (Deser et al., 2012). The validation statistics for LMR v2.0 and LMR v2.1 are nearly identical (Figure S4 in the Supporting Information S1). However, LMR v2.1 is better correlated with observations, and thus we focus on v2.1 in the analyses that follow. Both LMR v2.1 and PHYDA overestimate SSTA amplitude along the equatorial Pacific for El Niño events (Figures S2 and S3 in the Supporting Information S1). But in general, PHYDA reconstructs SSTA patterns with reduced bias and a closer match to observations in the eastern equatorial Pacific compared to LMR (Figures S2 and S3 in the Supporting Information S1).

To ensure our results are robust to the difference in year averaging choices of LMR and PHYDA, we analyzed SST and precipitation data from CESM-LME (Otto-Bliesner et al., 2016) using both annual-mean methods. The results indicate differences are negligible in the precipitation patterns, despite the use of different annual averaging windows (Figure S5 in the Supporting Information S1). Thus, we assert the main differences between the two DA products are not an artifact of the averaging window, but likely result from different choices in the reconstruction processes, such as use of different proxy system models and model bias correction methods (the latter of which is employed in PHYDA but not LMR, Steiger et al. (2018); Tardif et al. (2019)).

The methods used to partition CP and EP El Niño events process SST data differently, which might cause distinct expressions of SSTA patterns and indices. To evaluate the impact of these differences, we compared the CP and EP El Niño SSTA patterns for the 20th century in both DA products to HadISST (Figures 1 and 2), evaluating the three regional SST-based methods (Niño 3–4, CP-EP and C and E, see Section 2.2.2). Correlation coefficients (R) for each index are reported in Table 1. The Niño 3–4 and C and E methods in both DA products generally capture observed characteristics of CP and EP El Niño events in terms of SSTA patterns (Figures 1 and 2) and index correlations with observations ($R > 0.6$, $P < 0.05$, Table 1). Both DA products show stronger warming along the equator in CP and EP El Niño SSTA patterns compared to observations for the Niño 3–4 and C and E method (panels d, f, j, i in Figures 1 and 2). Warming maxima are shifted to the west in reconstructed EP El Niño SSTA patterns compared to HadISST (a known feature of CCSM/CESM and other climate models, Capotondi (2013)). In addition, for both the Niño 3–4 and C and E methods, CP and EP El Niño patterns in both reconstructions are similar to one another and not as distinct as patterns derived from HadISST. This is potentially due to the fact that CP and EP El Niño events are not adequately distinguished because of spatial biases in LMR and PHYDA's ENSO SSTA reconstructions (Figures S2 and S3 in the Supporting Information S1).

By contrast, the CP-EP method does not properly partition CP and EP El Niño SSTA patterns in paleo-reanalysis data (panels b, e, h, k in Figures 1 and 2). The SST patterns are poorly correlated with observations ($R < 0.5$, Table 1). EP El Niño SSTAs produced by this method are not readily identifiable El Niño-like patterns in LMR (Figures 2b and 2e), and the CP El Niño pattern in PHYDA exhibits weaker SST warming than that of HadISST (Figures 1h and 1k). The large discrepancies between observations and the DA products using the CP-EP method can be attributed to the relatively weak correlation of the Niño 1 + 2 index in reconstructions and observations (Figure S4 in the Supporting Information S1), which is likely driven by biases in the coastal upwelling simulated in the CCSM/CESM model priors (Deser et al., 2012); the CP-EP method is the only method that employs the Niño 1 + 2 index for CP and EP definitions. In addition, as the variance of the SST ensemble mean declines back in time in the DA products, especially for LMR (Figure S1 in the Supporting Information S1), uncertainties in

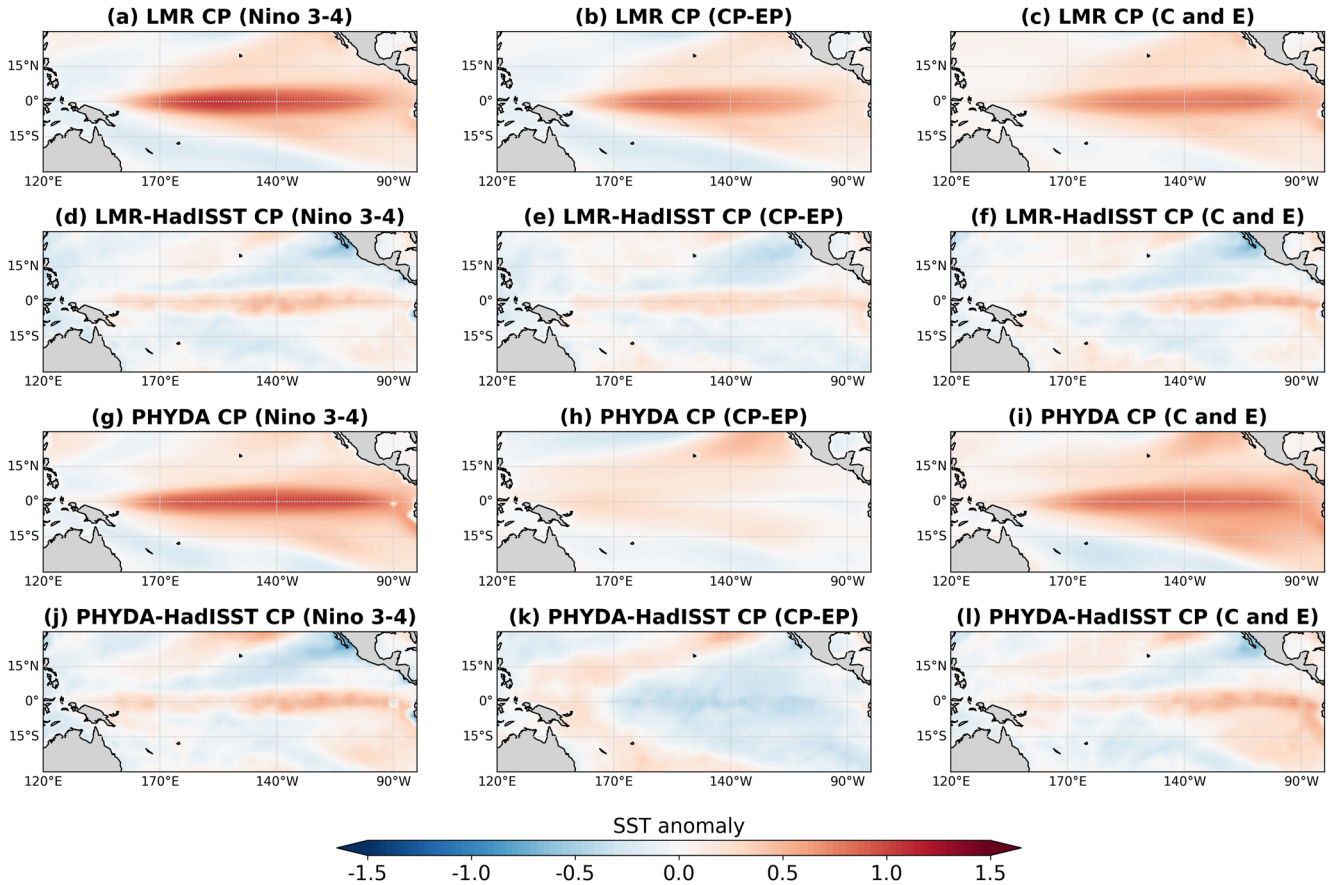

Figure 1. Reconstructed Central Pacific (CP) El Niño SSTA (°C) patterns in (a–f) Last Millennium Reanalysis (LMR) and (g–l) Paleo Hydrodynamics Data Assimilation (PHYDA) during the 20th century based on the Niño 3–4, CP-EP, and C and E methods. The differences between LMR/PHYDA and Hadley center SST (HadISST) during the 20th century are shown as difference maps (d, e, f, j, k, l).

the Niño 1 + 2 index reconstructed by DA products increases. These uncertainties are likely propagated when we remove the 1000-year based regression of the Niño 1 + 2 index onto SSTA, so the CP-EP method may result in larger biases in the calculation of the CP and EP index.

In general, both reconstructions are well correlated with observed ENSO characteristics (Figures S2 and S3 in the Supporting Information S1) and thus are appropriate tools for diagnosing ENSO changes over the LM. The expression of CP and EP El Niño events is dependent on the definition method used (Figures 1 and 2). Thus, in the text that follows, we consider only the Niño 3–4 and C and E methods for classifying CP and EP El Niño events and associated hydroclimate teleconnections in North America.

3.2. Frequency and Amplitude of CP and EP El Niño Over the Last Millennium

We first evaluate the frequency and amplitude changes of CP and EP El Niño during the LM, using the Niño 3–4 and C and E methods (Section 2.2.2). Figure 3 shows the frequency of (a) CP El Niño, (b) EP El Niño, and (c) the ratio of CP to EP El Niño (CP/EP) in 50-year windows in LMR and PHYDA. In general, CP El Niño events occur more frequently than EP El Niño events (at a rate of ∼10 out of every 50 years, while EP El Niño events occur at a rate of ∼5 out of every 50 years). The CP/EP ratio change highlights several time periods with more active CP El Niño events (Figures 3e and 3f, gray shading). However, these periods are generally inconsistent in timing between LMR and PHYDA and inconsistent amongst CP or EP definition methods. Although the CP/EP ratios for both LMR and PHYDA indicate increased recurrence of CP El Niño in the 20th century compared to the 19th century, equivalent or even higher ratios during other periods in the LM (Figures 3e and 3f) suggest that the frequency changes of CP El Niño in the 20th century are not necessarily anomalous in the context of the LM,

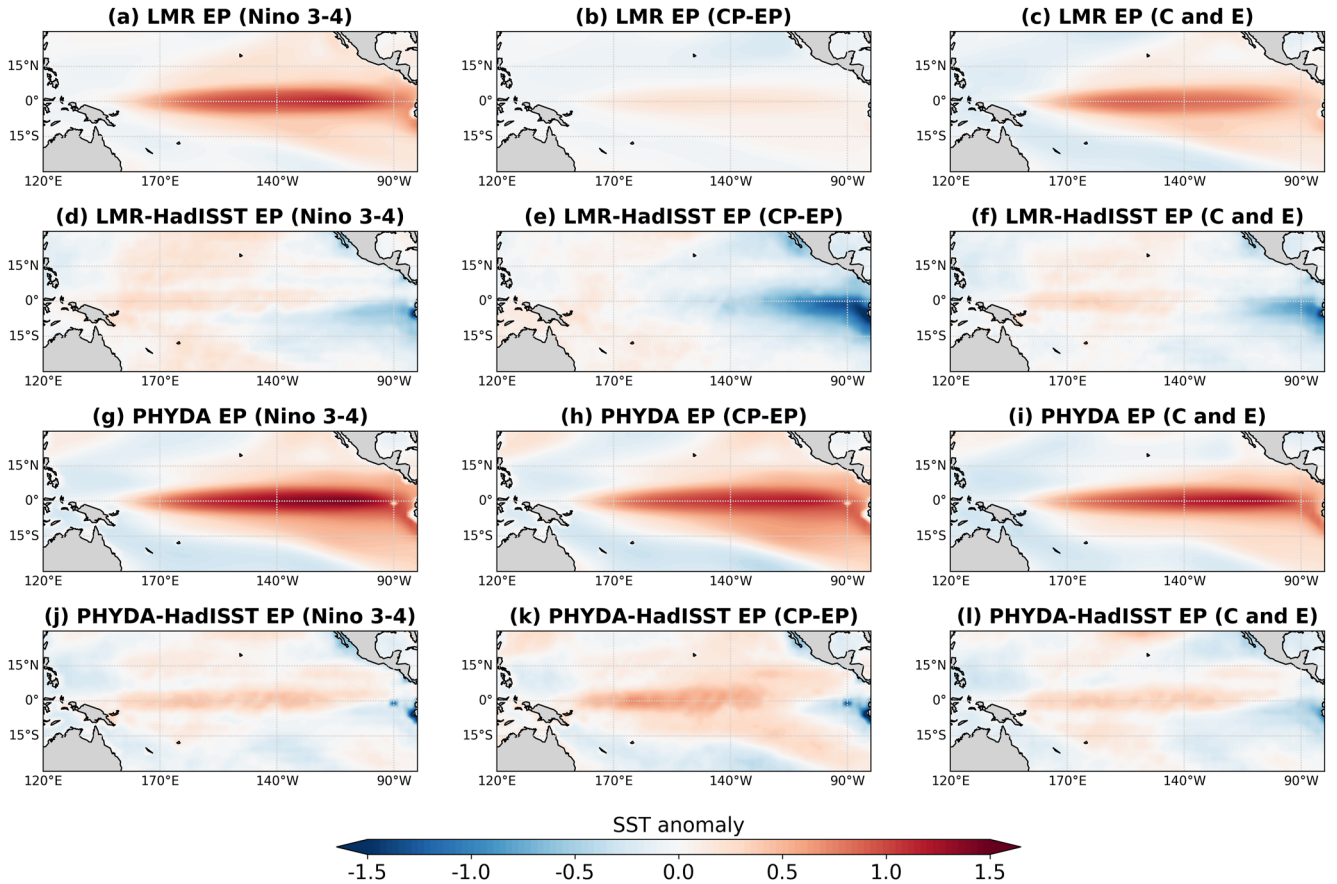

Figure 2. Same as Figure 1 but for EP El Niño.

and can be attributed to the natural variability of CP/EP on multi-centennial timescales. As a sensitivity test, we used 30-year and 70-year windows to evaluate the CP and EP El Niño frequency changes over the LM; the results are consistent across all three choices of averaging window size (Figures S6 and S7 in the Supporting Information S1). Importantly, these frequency results contrast with previous work evaluating paleoclimate records, which suggested a significant increase in the frequency of CP El Niño in the 20th century compared to previous centuries attributable to anthropogenic warming (Freund et al., 2019; Liu et al., 2017).

To test the sensitivity of the reconstructed changes in event frequency to proxy availability back in time (Figure S1 in the Supporting Information S1) and the impact of North American (NA) proxy records on El Niño SST reconstructions, we reproduced the step plots of CP and EP frequency using an LMR fixed-proxy reconstruction and the LMR experiment withholding all NA proxy records (Section 2.1.1). In the fixed-proxy reconstruction, the frequency changes differ from the full LMR (shown in Figure 3) but still yield natural variability on multi-centennial timescales (Figure S8 in the Supporting Information S1). Thus, the frequency changes of CP and EP El Niño through time cannot be solely explained by changing proxy density. In the second sensitivity experiment withholding NA proxies, event frequencies change differently compared to the full-network reconstructions in LMR and PHYDA; specifically, the variability of the CP/EP ratio decreases, and the frequency of CP El Niño using the Niño 3–4 method shows a significant increase in the 20th century. However, again, the results still exhibit internal variability throughout the LM (Figure S9 in the Supporting Information S1), further indicating that natural variability strongly influences multi-centennial frequency changes in CP and EP El Niño events.

Table 1
Temporal Correlation Coefficients (R) for Different Indices Between Reconstructions (LMR and PHYDA) and HadISST Under Different Definition Methods Partitioning CP and EP El Niño Variability During the 20th Century. (All Correlations Are Significant at the 95% Confidence Level)

Method	Niño 3–4		CP-EP		C and E	
El Niño type	CP	EP	CP	EP	CP	EP
LMR v2.1	0.85	0.75	0.44	0.30	0.63	0.63
PHYDA	0.74	0.76	0.29	0.37	0.70	0.62

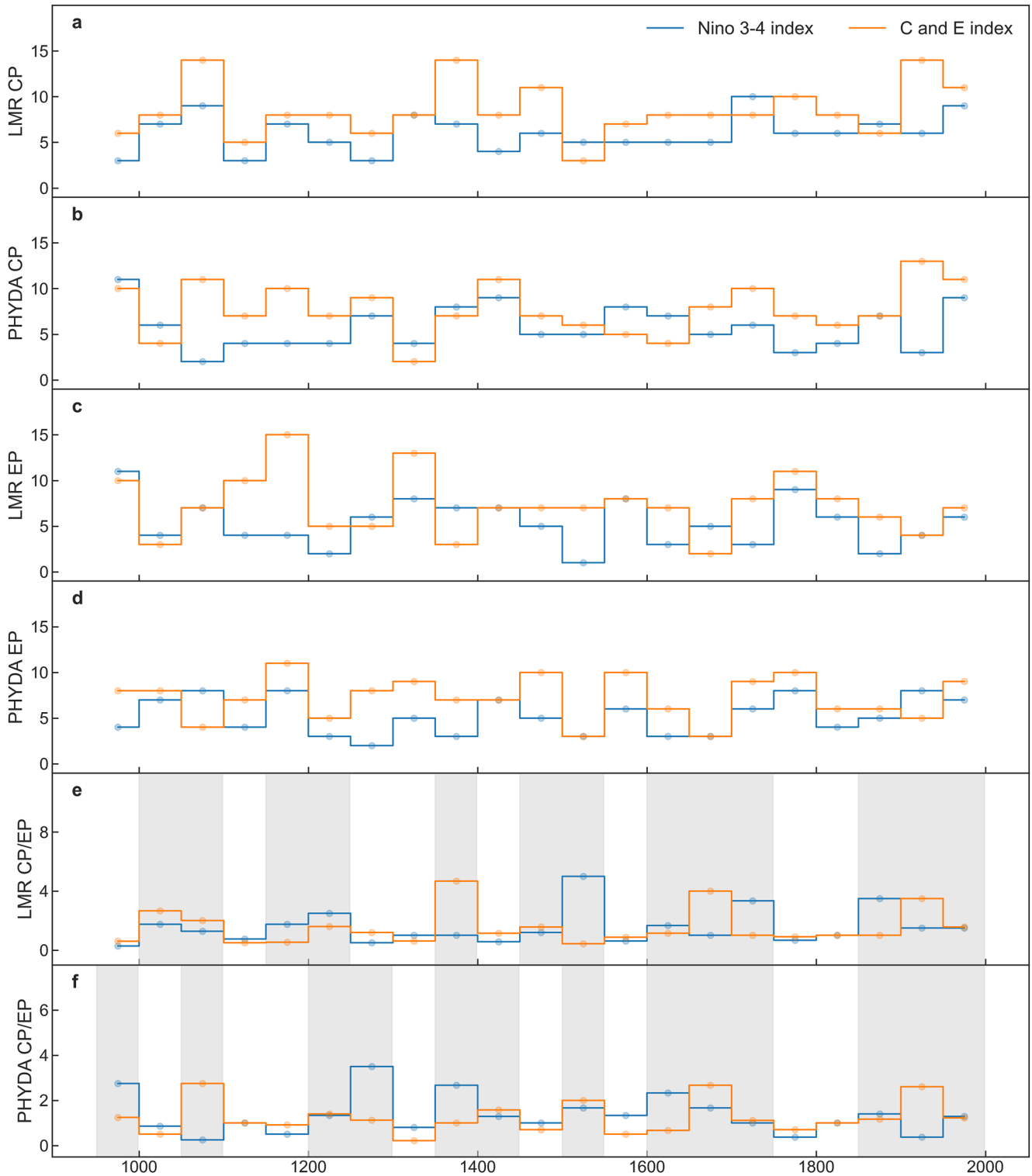

Figure 3. Central Pacific (CP) and Eastern Pacific (EP) El Niño event frequency (number/50 years) over the LM for Last Millennium Reanalysis (LMR) (a) and Paleo Hydrodynamics Data Assimilation Product (PHYDA) (b) CP frequency, LMR (c) and PHYDA (d) EP frequency and the ratio of CP to EP in LMR (e) and PHYDA (f). All frequencies are number of events per 50 years based on the two definition methods (Niño 3–4 and C and E). Shading in (e) and (f) represents time periods when the average ratio given by both methods is above 1 (CP frequency > EP frequency).

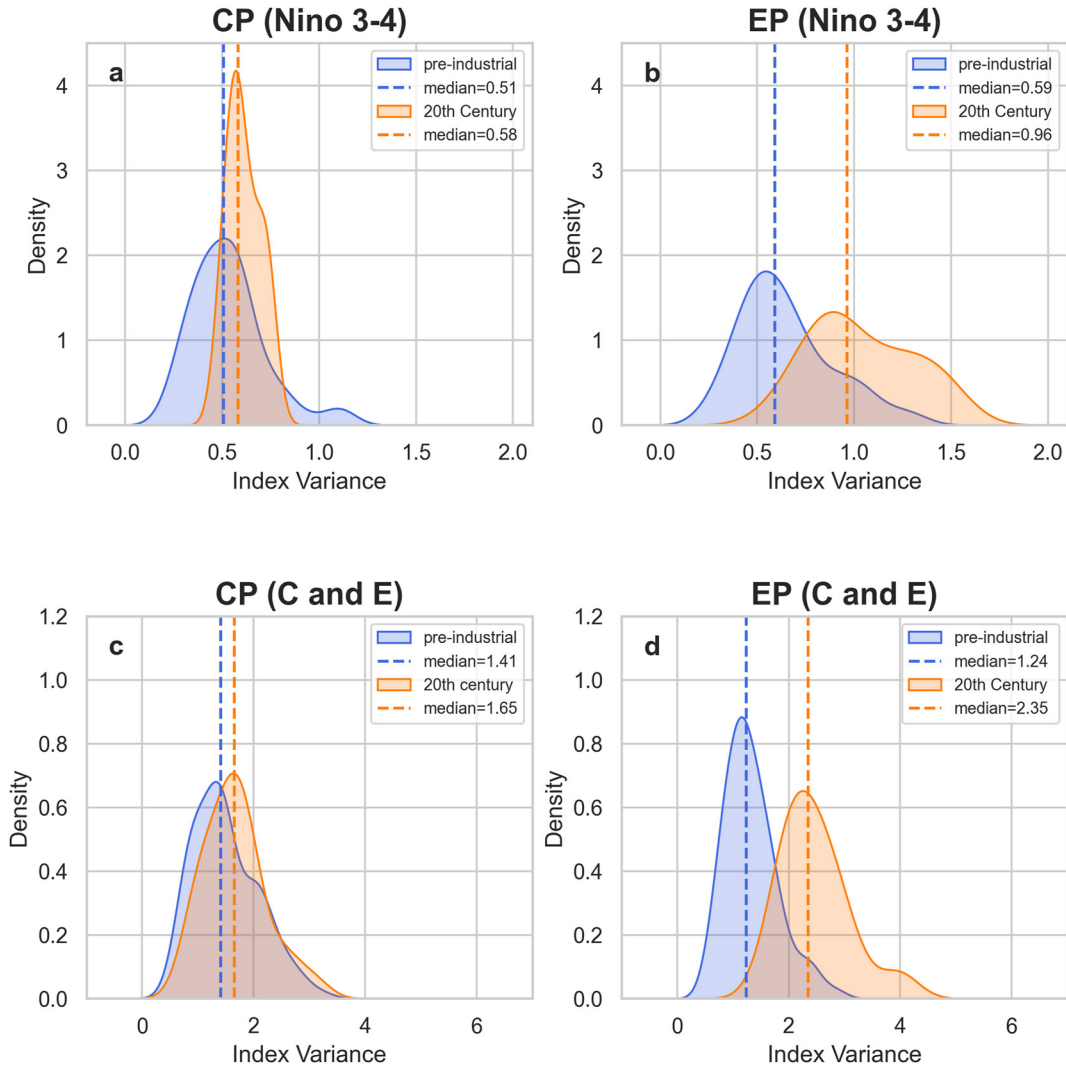

Figure 4. Probability density functions (PDFs) of indices based on Paleo Hydrodynamics Data Assimilation Product (PHYDA) data for (a) Central Pacific (CP) and (b) Eastern Pacific (EP) El Niño from the Niño 3–4 method, (c) CP and (d) EP El Niño from the C and E method during the pre-industrial and the 20th century. Dashed lines represent the medians of the distribution for different time periods.

In addition, we examine changes in the amplitude of CP and EP El Niño, an important control on teleconnection precipitation (Capotondi et al., 2015; Hoell et al., 2016). We compare the pre-industrial (1000–1850 C.E.) event variance of CP and EP El Niño to event variance during the 20th century to estimate the impact of climatic mean state changes on El Niño events. Given that the ENSO variance reduction in PHYDA is much less than that of LMR (Figure S1 in the Supporting Information S1), hereafter, we focus our discussion on the results produced using PHYDA (Figure 4). The probability density functions (PDFs) for CP and EP El Niño events during these two time periods are computed as a metric for event strength. Differences in the PDFs between the pre-industrial and the 20th century vary by definition method. However, both the Niño 3–4 and C and E methods show a significant increase ($p < 0.005$, Wilcoxon rank-sum test) in the amplitude of EP El Niño from the pre-industrial to the 20th century (Figures 4b and 4d) and very little change in the amplitude of CP El Niño (Figures 4a and 4c). Note that there are significant changes between the pre-industrial and the 20th century for both CP and EP El Niño in LMR (Figure S10 in the Supporting Information S1). Only the C and E method indicates similar CP and EP El Niño variance for both PHYDA and LMR (Figure 4 and S10 in the Supporting Information S1).

To assess the impact of proxy availability back in time (Figure S1 in the Supporting Information S1), we performed the same PDF analyses for the LMR fixed-proxy network reconstruction (Section 2.1.1). The results

(Figure S11 in the Supporting Information S1) yield similar PDFs of CP and EP El Niño variance changes (i.e., increased EP El Niño variance and no change in CP El Niño variance) when compared against PHYDA's results (Figure 4). This consistency provides support for the conclusion that these variance changes are not just based on changing proxy network density through time, yielding confidence in the robustness of our result. In sum, these analyses show that the amplitude of EP El Niño events increases significantly in the 20th century compared with the LM, while CP El Niño variance remains unchanged.

3.3. North American Hydroclimate Patterns and ENSO Diversity Over the Last Millennium

ENSO's impacts on extreme hydroclimate events (i.e., droughts and floods) across North America have been evaluated in previous work (Griffin & Anchukaitis, 2014; Munoz & Dee, 2017; Seager & Hoerling, 2014, and many others). To investigate in detail how hydroclimate events respond to distinct El Niño SSTA patterns, the methodology described in Sections 2.2.2 and 2.2.3 are applied to (a) differentiate CP and EP El Niño events throughout the LM and (b) extract corresponding maps of hydroclimate patterns over North America.

Composites of CP and EP El Niño SST and normalized PDSI anomalies (Figure 5) indicate that the spatial patterns of PDSI anomalies for CP or EP El Niño are generally consistent in both reconstructions and using both definition methods. The pattern correlations for the two methods ($R > 0.9$ for PHYDA, $R > 0.7$ for LMR) and between two DA products ($R > 0.53$ for CP El Niño, $R > 0.75$ for EP El Niño) are all significant at the 95% confidence level. We selected three key regions for documenting changes in hydroclimate based on both previous work (Herweijer et al., 2007) and by selecting dominant regions that exhibit large differences in hydroclimate across the U.S.: northwest (NW; 42°-50°N, 125°-115°W), eastern-to-central (E-Central; 30°-50°N, 100°-70°W), and southwest (SW; 30°-43°N, 115°-107°W). The NW and E-Central U.S. show decreased PDSI during CP El Niño events, and increased PDSI during EP El Niño events, while the SW U.S. shows increased PDSI during both types of El Niño events. These patterns are generally consistent with CP and EP El Niño hydroclimate conditions based on PDSI derived from observations (Figure S12 in the Supporting Information S1) and documented in previous work (Barsugli & Sardeshmukh, 2002; Weng et al., 2009). Dry conditions in the E-Central U.S. are more intense in the reconstructions compared to observations (Figure S12 in the Supporting Information S1); E-Central U.S. drought patterns during CP El Niño events in the LMR extend further south (covering areas along the Gulf of Mexico) compared to PDSI anomaly patterns in PHYDA (Figures 5a and 5e). Wet anomalies across the E-Central U.S. during EP El Niño events are the largest for LMR using the C and E method (Figures 5b, 5d, 5f and 5h). In addition, PHYDA reconstructs wetter conditions in the SW U.S. during CP El Niño events compared to CP El Niño (Figures 5c, 5d, 5g, and 5h), consistent with observations (Figure S12 in the Supporting Information S1). In general, the hydroclimate patterns for both DA products and for both methods yield a set of consistent results: (a) drier conditions during CP El Niño events and wetter conditions during EP El Niño events in the NW and E-Central U.S.; and 2) wetter anomalies across the SW U.S. for both CP and EP El Niño events.

Given the multi-decadal changes in the frequency and intensity of EP and CP El Niño events discussed in Section 3.2, we note that teleconnections and their impacts on hydroclimate patterns are likely non-stationary over the LM. Expanding on the composite characteristics given in Figure 5, we computed the temporal variability (step plot) and hydroclimate PDFs for three key regions (the SW, NW and E-Central U.S.) in Figure 6. We opted to focus our analyses on the C and E method given that this method exhibits more consistent CP and EP El Niño statistics and associated hydroclimate patterns between DA products (Section 3.2, Figure 5). Figure 6 shows that temporal changes in regional PDSI are not consistent in LMR and PHYDA; changes in teleconnection strength for CP and EP El Niño events are variable in all regions (Figures 6a, 6c, and 6e), indicating nonstationarity in El Niño teleconnections over the LM. In addition, increased CP El Niño teleconnection strength does not always temporally align with strengthened EP or all El Niño teleconection periods (Figures 6a, 6c, and 6e). However, in general, the SW U.S. experiences wetter conditions during both CP and EP El Niño events; the NW and E-Central U.S. experience drier conditions during CP El Niño events, and wetter conditions during EP El Niño events despite differences in teleconnection strength. These features are consistent with the PDFs shown in the right panel of Figure 6, which show that the SW U.S. shifts toward wetter conditions during both CP and EP El Niño events (Figure 6b); the NW and E-central U.S. shift toward dry conditions during CP El Niño but wet conditions during EP El Niño (Figures 6d and 6f). Although the spread in the PDFs in Figure 6 shows that the moisture supply in North America can be variable and even opposite in sign compared to the average, the shifts in PDSI in these selected regions are consistent with the mean hydroclimate patterns associated with certain CP and EP

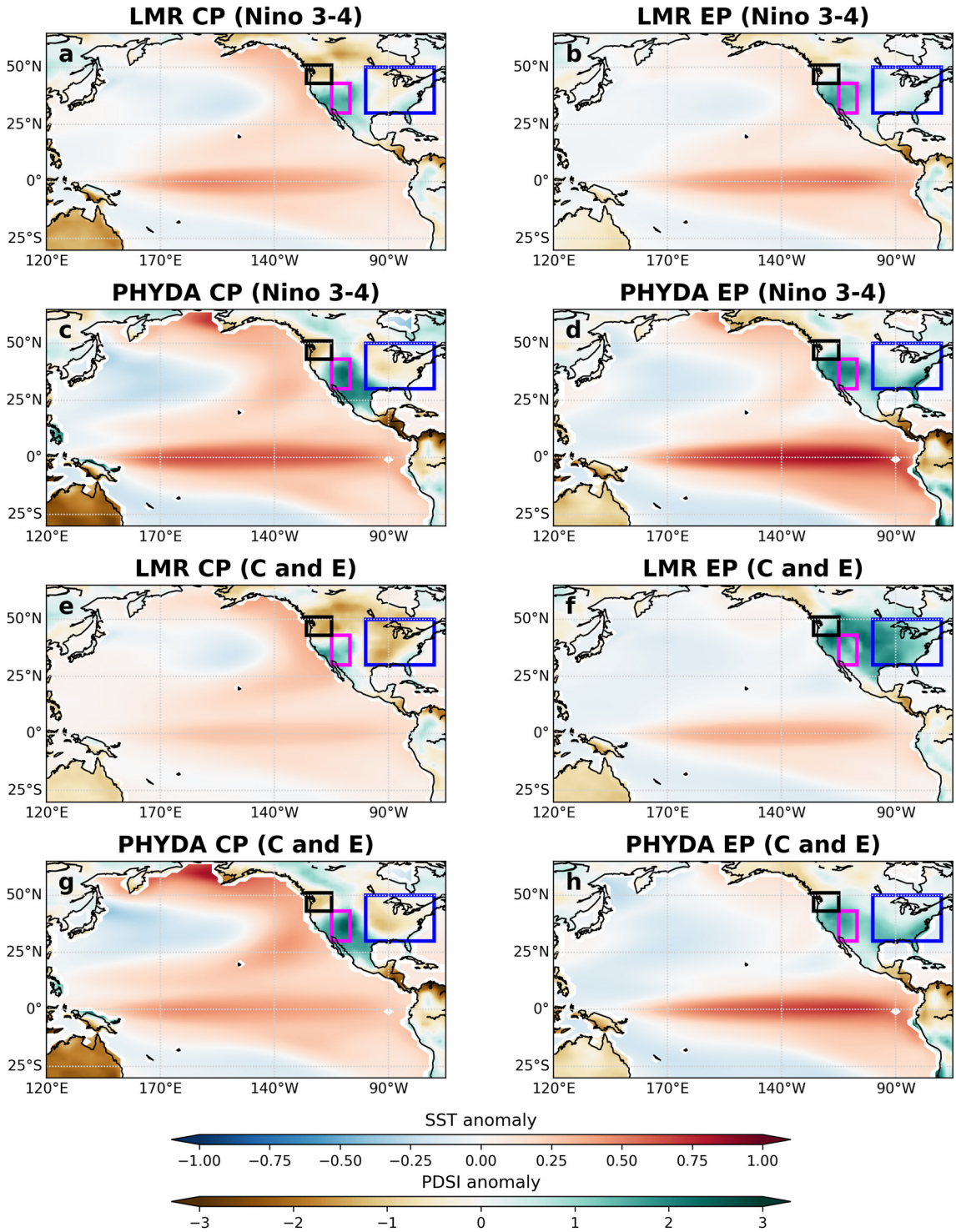

Figure 5. Maps showing composites of sea surface temperature anomalies (SSTA) (°C) and PDSI anomaly (unitless) of Last Millennium Reanalysis (LMR) and Paleo Hydrodynamics Data Assimilation Product (PHYDA) over the LM. (a, b) LMR's and (c, d) PHYDA's SSTA and PDSI anomaly composites patterns of Central Pacific (CP) and Eastern Pacific (EP) El Niño for Niño 3–4 method. (e, f) LMR's and (g, h) PHYDA's SSTA and PDSI anomaly composites for the C and E method. Red boxes represent the region used for the southwestern (SW) U.S.; black boxes encapsulate the northwestern (NW) U.S.; blue boxes encapsulate the eastern-central (E-central) U.S.

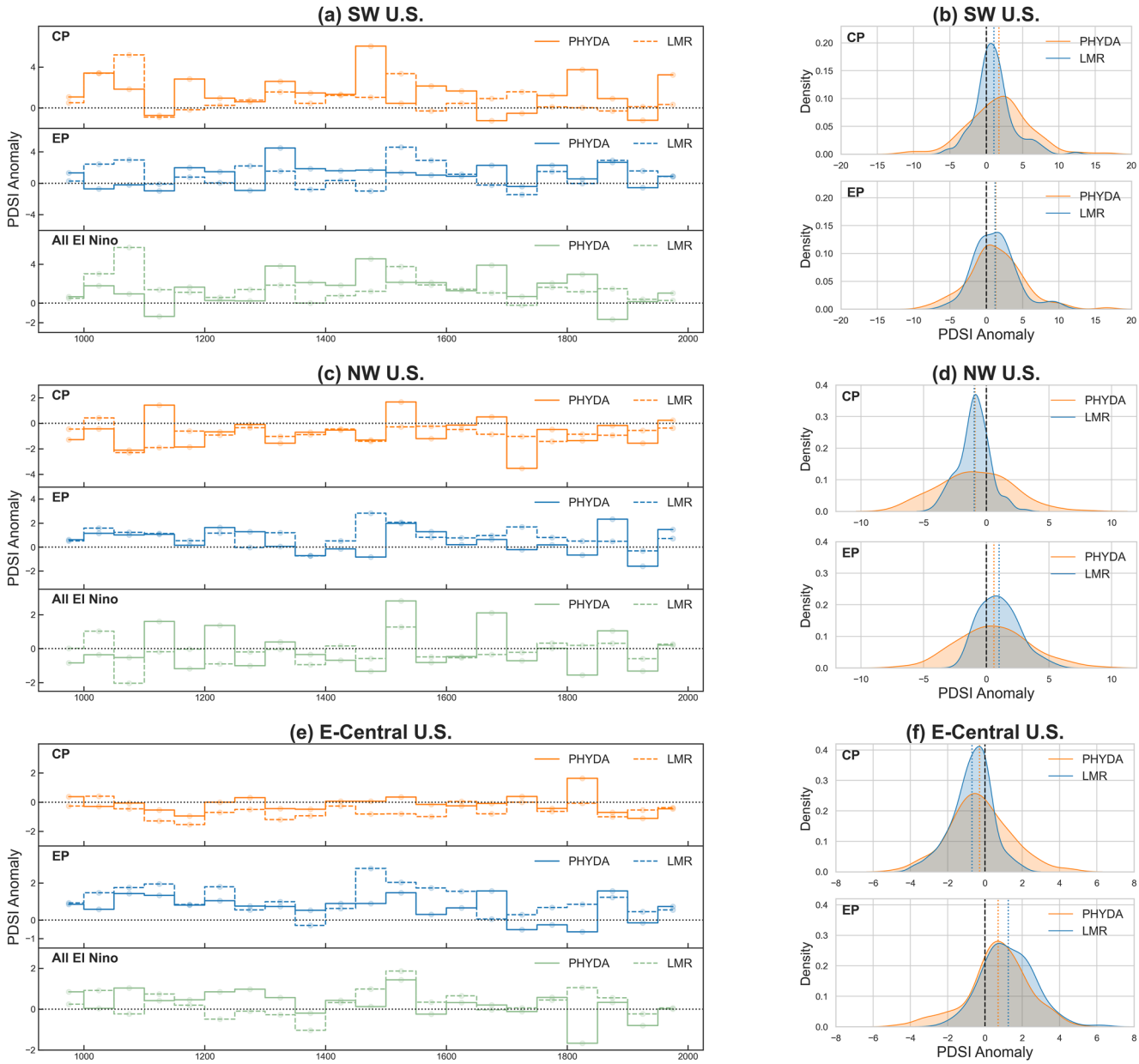

Figure 6. Temporal changes in Last Millennium Reanalysis (LMR's) and Paleo Hydrodynamics Data Assimilation Product's (PHYDA's) PDSI anomalies (unitless) for three key regions during the LM. Central Pacific (CP) and Eastern Pacific (EP) El Niño events are defined based on the C and E method. PDSI anomaly changes of CP, EP and all El Niño events (in 50-year window averages) for LMR and PHYDA in regions of (a) SW U.S., (c) NW U.S. and (e) E-Central U.S. PDFs of PDSI anomaly of CP and EP El Niño events in regions of (b) SW U.S., (d) NW U.S. and (f) E-Central U.S. All black dotted lines represent a neutral (0) PDSI anomaly. Dashed lines in (b), (d) and (f) represent the average of the distribution.

El Niño states in Figure 5. The shifts in the PDFs are weaker using the Niño 3–4 method compared to the C and E method, though consistent moisture conditions are evident during the two types of El Niño events for all three regions (Figure S13 in the Supporting Information S1).

To extend our comparison of CP and EP El Niño SST amplitudes in the pre-industrial and the 20th century (Figure 4), we compared the strength of CP and EP teleconnections during these two time periods (Figure 7). Here, we primarily present PHYDA's PDFs of scaled PDSI anomalies derived from the C and E method. The teleconnections exhibit large temporal variability (Figure 6); thus, the regional teleconnection changes are not consistent, and depend jointly on region and El Niño type. The changes in PDSI anomalies are not significant (considering all regions). The strength of the teleconnections remains unchanged between the pre-industrial and

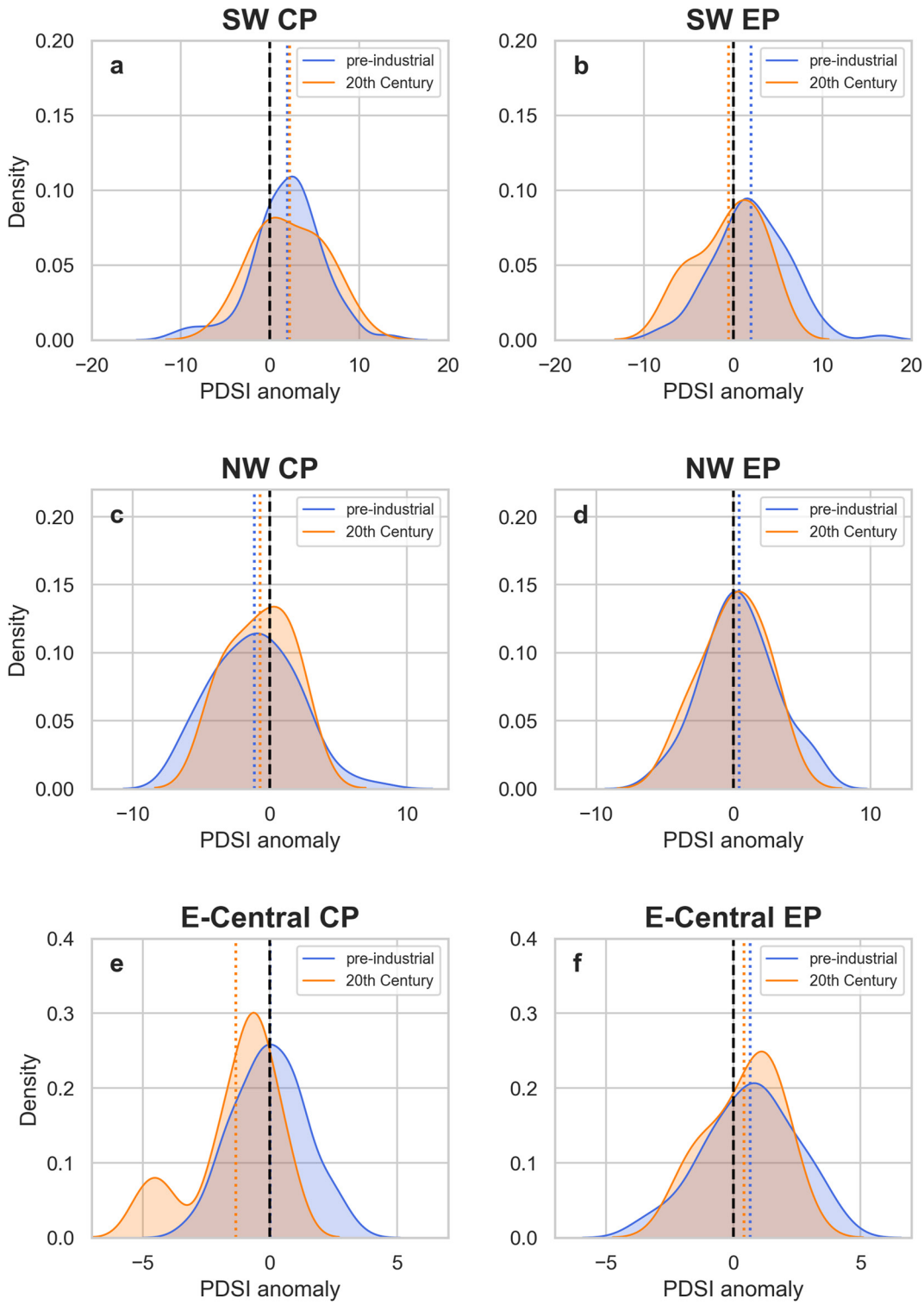

Figure 7. PDFs of PHYDA's PDSI anomaly (unitless) during the pre-industrial (blue lines) and the 20th century (orange lines) for (a) SW CP, (b) SW EP, (c) NW CP, (d) NW EP, (e) E-Central CP and (f) E-Central EP, based on C and E method. All black dashed lines represent a neutral (0 PDSI anomaly. Dotted lines represent the average of the distribution.

the 20th century in the SW U.S. during CP El Niño events and the NW U.S. during EP El Niño events (Figures 7a and 7d). The PDSI anomalies decrease slightly in the 20th century for the NW U.S. during CP El Niño events and for the SW and E-Central U.S. during EP El Niño events compared to the pre-industrial (Figures 7b, 7c, and 7f). Only the E-Central U.S. shows an increased teleconnection strength during CP events from the pre-industrial to the 20th century (Figure 7e). SST variance of CP El Niño remains unchanged in the 20th century (Figure 4), but the teleconnection during CP El Niño events show unchanged, increased, and decreased strength compared to the pre-industrial in the SW, E-Central, and NW regions, respectively (Figures 7a, 7c, and 7e). The significantly increased EP El Niño SST amplitude (Figure 4) does not result in strengthened hydroclimate teleconnections from the pre-industrial to the 20th century (Figures 7b, 7d, and 7f). The shifts in PDFs of LMR's normalized PDSI anomalies are similar to PHYDA's PDFs; however, CP El Niño teleconnections in the E-Central U.S. between the pre-industrial and the 20th century remain unchanged (Figure S14 in the Supporting Information S1). Taken together, the main conclusion stands: teleconnection strength is independent of El Niño SST variance, consistent with the results of S. Dee et al. (2020).

In general, teleconnection strength varies over time and varies independently from El Niño variance changes. However, consistent shifts in the PDSI anomalies for CP or EP El Niño events may prove informative for future prediction of regional hydroclimate conditions. Furthermore, average hydroclimate patterns are subject to change as a function of mean SSTA changes over time (S. Dee et al., 2020).

4. Discussion

This work investigates changes in the frequency of different SST patterns associated with CP and EP El Niño events (or El Niño "flavors") over the LM, and evaluates patterns of hydroclimate teleconnections over North America corresponding to each El Niño flavor to diagnose how teleconnections evolved over the LM. Such information has implications for the predictability of hydroclimate conditions associated with CP and EP El Niño events.

Differentiation of ENSO diversity in terms of CP versus EP El Niño events is largely method- and data-dependent. In general, all methods differ in their identification of El Niño flavors. For example, the observed 1997/1998 strong EP El Niño event is partitioned as both a CP and EP El Niño event in all methods except for the C and E method. The uncertainties associated with methods of event classification underscore the risk of employing one single method to characterize El Niño SSTA patterns over time, especially when applied to paleoclimate reconstructions, which are imperfectly resolved in time and space. Our results also suggest that, for more accurate predictions, the binary system of CP versus EP El Niño may not offer robust constraints on the hydroclimate patterns that emerge for a given El Niño event in paleoclimate DA products, which are also spatially complete and constrained by observations. A recent study documented that El Niño events with weak zonal SSTA gradients may result in ocean-atmosphere decoupling, which impacts extratropical precipitation (Hu et al., 2020). The similarity between such "uncoupled" El Niño warming events and CP El Niño events in terms of both SSTA patterns and hydrological impacts indicates that the spatial details of event-to-event ocean-atmosphere coupling and sensitivity to event-based SST patterns remain underdetermined. While many classification methods of CP and EP El Niño do include full spatiotemporal information via EOF analyses, to improve prediction, we assert that rather than binary indices derived from regional SST, studies which consider the complexity of tropical Pacific SST pattern and its interaction with the atmosphere (i.e., the position of the convective threshold (Okumura, 2019; Patricola et al., 2020)) are needed, especially for precipitation prediction.

Despite the differences between the various methods and data products, we identify several consistent changes in the frequency and amplitude of CP and EP El Niño events and corresponding hydroclimate patterns over North America. Both the Niño 3–4 and the C and E methods applied to LMR and PHYDA show large variability in CP/EP El Niño event frequency during the LM (Figure 3). In contrast, recent work using coral reconstructions documented an unprecedented increase in CP El Niño recurrence in the 20th century, and attribute these changes to anthropogenic warming (Freund et al., 2019; Yeh et al., 2009). Our results suggest that the increase of CP El Niño event frequency in the 20th century is not anomalous compared to other centuries during the LM, and can be attributed to the natural variability of CP and EP El Niño occurrence, consistent with work of Newman et al. (2011) and Yeh et al. (2011). The differences of CP and EP El Niño recurrence might be attributed to the different proxy networks used for past SST reconstructions; Freund et al. (2019) only used tropical coral

records, while the DA products used in our analysis reconstruct climate based on global networks of paleoclimate records (e.g., adding tree-ring records over North America). DA reconstructions which test sensitivity to proxy network and type (i.e., coral-only) would be needed to further diagnose the discrepancy (e.g., Sanchez et al., 2021). However, in agreement with Freund et al. (2019), we do find that increased EP El Niño strength in the 20th century emerges using both methods (Figure 4).

While the impacts of LM external forcing on ENSO and its hydroclimate teleconnections (i.e., volcanic forcing) are well-documented (Stevenson et al., 2017; Stevenson et al., 2018; S. G. Dee et al., 2020; Zhu et al., 2020; Tejedor et al., 2021a, 2021b; Sanchez et al., 2021, and many others), our analysis suggests multi-decadal changes in El Niño teleconnections over North America are indicative of large and unforced internal variability, including across the 20th century. For example, as shown in Figure 6, strengthening teleconnections do not necessarily synchronize with strengthened El Niño SSTs (S. Dee et al., 2020). Teleconnections exhibit large natural multi-decadal- to centennial-scale variability during the LM, a result consistent with previous work evaluating teleconnections in model simulations (Coats et al., 2013; Lewis & LeGrande, 2015). The temporal changes in teleconnection strength do not show a shift toward enhanced hydroclimate conditions in the 20th century, for example, alongside larger EP El Niño variance (Figures 4 and 7). That said, CP and EP El Niño hydroclimate conditions in North America do show generally consistent changes in moisture supply over the LM in both DA products (Figures 5 and 6). For example, in the E-Central and NW U.S., a shift toward drier (wetter) conditions occurs during CP (EP) El Niño events. Moisture supply in the SW U.S. increases for both El Niño types. Although the magnitude of hydroclimate response to CP and EP El Niño varies substantially on multi-decadal timescales, the signs of those anomalies are consistent through the last millennium in the three U.S. regions evaluated here. Overall, the consistency between the two paleoclimate reconstructions gives us confidence in the distinct hydroclimate response to CP and EP El Niño events.

We acknowledge several limitations of this work. Proxy records are fundamentally imperfect recorders of past climate variability and contain seasonal information biases. Additionally, the proxy networks used in the LMR and PHYDA decrease in size further back in time; this decrease in proxy information corresponds with an increase in the reconstruction uncertainties. An additional feature of data assimilation-based reconstructions is that as proxy information decreases, the reconstruction will drift closer to the mean climate model state, thereby reducing the time series variance of the ensemble mean (see Figure S1 in the Supporting Information S1) (Hakim et al., 2016; Tardif et al., 2019; Steiger et al., 2018). Uncertainties are also driven by the location and the spatial concentration of proxy records in different geographical areas; for example, there are far fewer proxy records in the Southern Hemisphere assimilated into the reconstructions (Steiger et al., 2018). The proxy data-driven changes in variance introduces uncertainties in distinguishing between CP and EP El Niño SSTA patterns (CP-EP method in Figures 1 and 2), CP and EP El Niño event frequency changes (e.g., Figures 3 and S6 in the Supporting Information S1), and CP and EP El Niño variance (e.g., Figures S10 and S11 in the Supporting Information S1). In addition, the use of different model priors in paleoclimate DA can have a large impact on the reconstructed SST and teleconnections (L. Parsons & Hakim, 2019; Amrhein et al., 2020). In particular, several studies have highlighted the exaggerated ENSO pattern in both CCSM4 and CESM; ENSO variance in the model exceeds that of the observations (Deser et al., 2012; Stevenson et al., 2016), and this enhanced ENSO response may amplify the DA sensitivity in teleconnected regions. Through the use of an LMR experiment that excluded North American proxy records in the DA reconstruction (Figure S9 in the Supporting Information S1), we confirmed that while the reconstruction still shows demonstrable internal variability throughout the LM, the North American records unsurprisingly add considerable information to the reconstruction in the tropical Pacific, and thus our results are highly sensitive to regional proxy information in teleconnected areas.

Given the impact of the model prior in reconstructing past ENSO and teleconnections, future work is needed to determine whether the characteristics of past CP and EP El Niño events and their hydroclimate responses reported here are robust to different model priors (L. A. Parsons et al., 2021). Furthermore, additional studies using a prior that incorporates the covariance structure of historical observations (e.g., reanalysis) could potentially reduce uncertainties in data assimilation-based reconstructions of past climate (Amrhein et al., 2020; Perkins & Hakim, 2020). Finally, as a guide for future work, we note that LMR and PHYDA were designed with different climate reconstruction goals in mind, which dictated their proxy selection choices. The PAGES2k Consortium proxy network chosen for LMR v2.1 is temperature-sensitive by design, while PHYDA includes hydroclimate-sensitive proxies in an effort to reconstruct ENSO and its hydroclimate response. Despite the different

networks employed in both reconstructions, our results show similarities, and such DA product inter-comparison is valuable for identifying consistent and robust features of El Niño and North American hydroclimate over the LM. Nonetheless, future work should consider the differences between currently available and forthcoming DA products to ensure the choice of reconstruction is well-aligned with the given scientific question.

5. Conclusions

As greenhouse gas concentrations in the atmosphere continue to increase, hydroclimate extremes are projected to intensify over North America (Collins et al., 2013; Kirtman et al., 2013; Masson-Delmotte et al., 2013). However, it remains unclear how ENSO teleconnections will modulate hydroclimate extremes in a warming climate (Stevenson, 2012). At present, projections of changes to ENSO hydroclimate teleconnections over the 21st century vary widely (Fasullo et al., 2018; Perry et al., 2020; Stevenson, 2012; Zhou et al., 2014). Given these distinct projections, future changes in teleconnection precipitation remain unclear for both El Niño types. Consistent hydroclimate shifts observed during CP versus EP El Niño events over the LM in the DA products provide important observational targets for Last Millennium simulations, and may prove useful for (a) ground-truthing model simulations of precipitation patterns over the US for different types of events, and (b) prediction of regional hydroclimate associated with CP or EP El Niño if the spatial SST pattern is known in advance.

Anthropogenic warming impacts on SST have been shown to be more conducive to CP El Niño generation in the 21st century, leading to increased CP El Niño event frequency in future projections (Lee & McPhaden, 2010; Yeh et al., 2009). If such model projections are correct, the frequency of hydroclimate extremes associated with CP El Niño events over North America will increase as well. The analysis presented here indicates that drought may become more frequent in the E-Central and NW U.S., while the SW U.S. may experience wetter conditions more often with increasing CP El Niño events.

Finally, hydroclimate anomalies modulated by ENSO teleconnections are clearly sensitive to the pattern of SST anomalies (Zhou et al., 2014; Xie, 2020; S. Dee et al., 2020; Patricola et al., 2020). If teleconnection (precipitation and temperature) strength and ENSO SST spatial expressions shift with background warming in the tropical Pacific, impacts will include changes in the spatial structure and recurrence of drought and heavy precipitation in the SW U.S., as well as changes in flooding regimes in the Mississippi and Ohio River Basins (Griffin & Anchukaitis, 2014; Seager & Hoerling, 2014; Munoz & Dee, 2017; S. Dee et al., 2020). These changes may be predictable. Research such as this, which characterizes ENSO diversity and corresponding hydroclimate impacts on extratropical regions, especially amidst ever-changing anthropogenic warming impacts, is a first step toward refining projections of changes in extreme events and their interactions with large-scale natural modes of climate variability.

Conflict of Interest

The authors declare no conflicts of interest relevant to this study.

Data Availability Statement

All of the DA product datasets used in this analysis are publicly available:LMR (https://atmos.uw.edu/~hakim/lmr/LMRv2/index.html and https://doi.org/10.5281/zenodo.5636999), PHYDA (https://doi.org/10.5281/zenodo.1198817), HadISST v1.1 (https://www.metoffice.gov.uk/hadobs/hadisst/data/HadISST_sst.nc.gz), Global PDSI (http://hydrology.princeton.edu/data/pdsi, Sheffield et al. (2006); Sheffield et al. (2012)), and CESM LME (https://www.earthsystemgrid.org/dataset/ucar.cgd.ccsm4.cesmLME.atm.proc.monthly_ave.html).

Acknowledgments
This work was supported by the National Oceanic and Atmospheric Administration (NOAA Award Number NA18OAR4310427) awarded to S.D. and by a graduate fellowship from the Department of Earth, Environmental, and Planetary Sciences at Rice University. This work was also supported under the National Science Foundation (NSF) under grants AGS-1805490 to N.S. and AGS-1805143 to S.S. This work was also supported in part by the Israel Science Foundation (ISF) award 2654/20. LAP acknowledges NASA GISS grant number 80NSSC19M0138 for funding support.

References

Amrhein, D. E., Hakim, G. J., & Parsons, L. A. (2020). Quantifying structural uncertainty in paleoclimate data assimilation with an application to the last millennium. *Geophysical Research Letters*, *47*(22), e2020GL090485. https://doi.org/10.1029/2020gl090485

Anderson, D., Tardif, R., Horlick, K., Erb, M., Hakim, G., Noone, D., & Steig, E. (2019). Additions to the last millennium reanalysis multi-proxy database. *Data Science Journal*, *18*(1). https://doi.org/10.5334/dsj-2019-002

Ashcroft, L., Gergis, J., & Karoly, D. J. (2016). Long-term stationarity of El Niño-southern oscillation teleconnections in southeastern Australia. *Climate Dynamics*, *46*(9–10), 2991–3006. https://doi.org/10.1007/s00382-015-2746-3

Ashok, K., Behera, S. K., Rao, S. A., Weng, H., & Yamagata, T. (2007). El Niño Modoki and its possible teleconnection. *Journal of Geophysical Research*, *112*(C11). https://doi.org/10.1029/2006jc003798

Barsugli, J. J., & Sardeshmukh, P. D. (2002). Global atmospheric sensitivity to tropical SST anomalies throughout the Indo-Pacific basin. *Journal of Climate*, *15*(23), 3427–3442. https://doi.org/10.1175/1520-0442(2002)015<3427:gastts>2.0.co;2

Breitenmoser, P. D., Brönnimann, S., & Frank, D. (2014). Forward modelling of tree-ring width and comparison with a global network of tree-ring chronologies. *Climate of the Past*, *10*(2), 437–449. https://doi.org/10.5194/cp-10-437-2014

Capotondi, A. (2013). ENSO diversity in the NCAR CCSM4 climate model. *Journal of Geophysical Research: Oceans*, *118*(10), 4755–4770. https://doi.org/10.1002/jgrc.20335

Capotondi, A., Wittenberg, A. T., Newman, M., Di Lorenzo, E., Yu, J.-Y., Braconnot, P., et al. (2015). Understanding ENSO diversity. *Bulletin of the American Meteorological Society*, *96*(6), 921–938. https://doi.org/10.1175/bams-d-13-00117.1

Cayan, D. R. (1980). Large-scale relationships between sea surface temperature and surface air temperature. *Monthly Weather Review*, *108*(9), 1293–1301. https://doi.org/10.1175/1520-0493(1980)108<1293:lsrbss>2.0.co;2

Changnon, S. A. (1999). Impacts of 1997-98 EI Niño-generated weather in the United States. *Bulletin of the American Meteorological Society*, *80*(9), 1819–1827. https://doi.org/10.1175/1520-0477(1999)080<1819:ioenog>2.0.co;2

Coats, S., Smerdon, J. E., Cook, B. I., & Seager, R. (2013). Stationarity of the tropical pacific teleconnection to North America in CMIP5/PMIP3 model simulations. *Geophysical Research Letters*, *40*(18), 4927–4932. https://doi.org/10.1002/grl.50938

Cobb, K. M., Charles, C. D., Cheng, H., & Edwards, R. L. (2003). El Niño/Southern Oscillation and tropical Pacific climate during the last millennium. *Nature*, *424*(6946), 271–276. https://doi.org/10.1038/nature01779

Collins, M., Knutti, R., Arblaster, J., Dufresne, J.-L., Fichefet, T., Friedlingstein, P., & Wehner, M. (2013). Long-term climate change: Projections, commitments and irreversibility [Book section]. In T. Stocker, et al. (Eds.), *Climate change 2013: The physical science basis. Contribution of working Group I to the fifth assessment report of the intergovernmental panel on climate change* (p. 1029–1136). Cambridge University Press. https://doi.org/10.1017/CBO9781107415324.024

Dee, S., Okumura, Y., Stevenson, S., & Di Nezio, P. (2020). Enhanced North American ENSO teleconnections during the little ice age revealed by paleoclimate data assimilation. *Geophysical Research Letters*, e2020GL087504. https://doi.org/10.1029/2020gl087504

Dee, S. G., Cobb, K. M., Emile-Geay, J., Ault, T. R., Edwards, R. L., Cheng, H., & Charles, C. D. (2020). No consistent ENSO response to volcanic forcing over the last millennium. *Science*, *367*(6485), 1477–1481. https://doi.org/10.1126/science.aax2000

Deser, C., Phillips, A. S., Tomas, R. A., Okumura, Y. M., Alexander, M. A., Capotondi, A., et al. (2012). ENSO and pacific decadal variability in the community climate system model version 4. *Journal of Climate*, *25*(8), 2622–2651. https://doi.org/10.1175/jcli-d-11-00301.1

Deser, C., Simpson, I. R., McKinnon, K. A., & Phillips, A. S. (2017). The Northern Hemisphere extratropical atmospheric circulation response to ENSO: How well do we know it and how do we evaluate models accordingly? *Journal of Climate*, *30*(13), 5059–5082. https://doi.org/10.1175/jcli-d-16-0844.1

Diaz, H. F., Hoerling, M. P., & Eischeid, J. K. (2001). ENSO variability, teleconnections and climate change. *International Journal of Climatology: A Journal of the Royal Meteorological Society*, *21*(15), 1845–1862. https://doi.org/10.1002/joc.631

Fasullo, J., Otto-Bliesner, B., & Stevenson, S. (2018). ENSO's changing influence on temperature, precipitation, and wildfire in a warming climate. *Geophysical Research Letters*, *45*(17), 9216–9225. https://doi.org/10.1029/2018gl079022

Freund, M. B., Henley, B. J., Karoly, D. J., McGregor, H. V., Abram, N. J., & Dommenget, D. (2019). Higher frequency of Central Pacific El Niño events in recent decades relative to past centuries. *Nature Geoscience*, *12*(6), 450. https://doi.org/10.1038/s41561-019-0353-3

Giese, B. S., & Ray, S. (2011). El Niño variability in simple ocean data assimilation (SODA), 1871-2008. *Journal of Geophysical Research: Oceans*, *116*(C2). https://doi.org/10.1029/2010jc006695

Griffin, D., & Anchukaitis, K. J. (2014). How unusual is the 2012-2014 California drought? *Geophysical Research Letters*, *41*(24), 9017–9023. https://doi.org/10.1002/2014gl062433

Hakim, G. J., Emile-Geay, J., Steig, E. J., Noone, D., Anderson, D. M., Tardif, R., & Perkins, W. A. (2016). The last millennium climate reanalysis project: Framework and first results. *Journal of Geophysical Research: Atmospheres*, *121*(12), 6745–6764. https://doi.org/10.1002/2016jd024751

Herweijer, C., Seager, R., Cook, E. R., & Emile-Geay, J. (2007). North American droughts of the last millennium from a gridded network of tree-ring data. *Journal of Climate*, *20*(7), 1353–1376. https://doi.org/10.1175/jcli4042.1

Hoell, A., Hoerling, M., Eischeid, J., Wolter, K., Dole, R., Perlwitz, J., & Cheng, L. (2016). Does El Niño intensity matter for California precipitation? *Geophysical Research Letters*, *43*(2), 819–825. https://doi.org/10.1002/2015gl067102

Hoerling, M. P., & Kumar, A. (1997). Why do North American climate anomalies differ from one El Niño event to another? *Geophysical Research Letters*, *24*(9), 1059–1062. https://doi.org/10.1029/97gl00918

Hu, Z.-Z., McPhaden, M. J., Kumar, A., Yu, J.-Y., & Johnson, N. C. (2020). Uncoupled El Niño warming. *Geophysical Research Letters*, *47*(7), e2020GL087621. https://doi.org/10.1029/2020gl087621

Johnson, N. C. (2013). How many ENSO flavors can we distinguish? *Journal of Climate*, *26*(13), 4816–4827. https://doi.org/10.1175/jcli-d-12-00649.1

Johnson, N. C., & Kosaka, Y. (2016). The impact of eastern equatorial Pacific convection on the diversity of boreal winter El Niño teleconnection patterns. *Climate Dynamics*, *47*(12), 3737–3765. https://doi.org/10.1007/s00382-016-3039-1

Kao, H.-Y., & Yu, J.-Y. (2009). Contrasting eastern-Pacific and central-Pacific types of ENSO. *Journal of Climate*, *22*(3), 615–632. https://doi.org/10.1175/2008jcli2309.1

Kirtman, B., Power, S., Adedoyin, J., Boer, G., Bojariu, R., Camilloni, I.2013Near-term climate change: Projections and predictability [book section], et al., et al. (Eds.), *Climate change 2013: The physical science basis. Contribution of working Group I to the fifth assessment report of the intergovernmental panel on climate change* (p. 953–1028). Cambridge University Press. https://doi.org/10.1017/CBO9781107415324.023

Kug, J.-S., & Ham, Y.-G. (2011). Are there two types of La Niña? *Geophysical Research Letters*, *38*(16). https://doi.org/10.1029/2011gl048237

Kug, J.-S., Jin, F.-F., & An, S.-I. (2009). Two types of El Niño events: Cold tongue El Niño and warm pool El Niño. *Journal of Climate*, *22*(6), 1499–1515. https://doi.org/10.1175/2008jcli2624.1

Landrum, L., Otto-Bliesner, B. L., Wahl, E. R., Conley, A., Lawrence, P. J., Rosenbloom, N., & Teng, H. (2013). Last millennium climate and its variability in CCSM4. *Journal of Climate*, *26*(4), 1085–1111. https://doi.org/10.1175/jcli-d-11-00326.1

Larkin, N. K., & Harrison, D. (2005a). Global seasonal temperature and precipitation anomalies during El Niño autumn and winter. *Geophysical Research Letters*, *32*(16). https://doi.org/10.1029/2005gl022860

Larkin, N. K., & Harrison, D. (2005b). On the definition of El Niño and associated seasonal average US weather anomalies. *Geophysical Research Letters*, *32*(13). https://doi.org/10.1029/2005gl022738

Lee, T., & McPhaden, M. J. (2010). Increasing intensity of El Niño in the central-equatorial pacific. *Geophysical Research Letters*, *37*(14). https://doi.org/10.1029/2010gl044007

Lewis, S. C., & LeGrande, A. N. (2015). Stability of ENSO and its tropical pacific teleconnections over the last millennium. *Climate of the Past*, *11*(10), 1347–1360. https://doi.org/10.5194/cp-11-1347-2015

Liu, Y., Cobb, K. M., Song, H., Li, Q., Li, C.-Y., & Nakatsuka, T. (2017). othersRecent enhancement of central Pacific El Niño variability relative to last eight centuries. *Nature Communications*, *8*, 15386. https://doi.org/10.1038/ncomms15386

Lloyd, J., Guilyardi, E., & Weller, H. (2011). The role of atmosphere feedbacks during ENSO in the CMIP3 models. Part II: Using AMIP runs to understand the heat flux feedback mechanisms. *Climate Dynamics*, *37*(7–8), 1271–1292. https://doi.org/10.1007/s00382-010-0895-y

Lloyd, J., Guilyardi, E., & Weller, H. (2012). The role of atmosphere feedbacks during ENSO in the CMIP3 models. Part III: The shortwave flux feedback. *Journal of Climate*, *25*(12), 4275–4293. https://doi.org/10.1175/jcli-d-11-00178.1

Lloyd, J., Guilyardi, E., Weller, H., & Slingo, J. (2009). The role of atmosphere feedbacks during ENSO in the CMIP3 models. *Atmospheric Science Letters*, *10*(3), 170–176. https://doi.org/10.1002/asl.227

Masson-Delmotte, V., Schulz, M., Abe-Ouchi, A., Beer, J., Ganopolski, A., González Rouco, J., & Timmermann, A. (2013). Information from paleoclimate archives [book section]. In T. Stocker, et al. (Eds.), *Climate change 2013: The physical science basis. Contribution of working Group I to the fifth assessment report of the intergovernmental panel on climate change* (p. 383–464). Cambridge University Press. https://doi.org/10.1017/CBO9781107415324.013

Munoz, S. E., & Dee, S. G. (2017). El Niño increases the risk of lower Mississippi River flooding. *Scientific Reports*, *7*(1), 1–7. https://doi.org/10.1038/s41598-017-01919-6

Newman, M., Shin, S.-I., & Alexander, M. A. (2011). Natural variation in ENSO flavors. *Geophysical Research Letters*, *38*(14). https://doi.org/10.1029/2011gl047658

Oke, P. R., Allen, J. S., Miller, R. N., Egbert, G. D., & Kosro, P. M. (2002). Assimilation of surface velocity data into a primitive equation coastal ocean model. *Journal of Geophysical Research: Oceans*, *107*(C9), 5–1. https://doi.org/10.1029/2000jc000511

Okumura, Y. M. (2019). ENSO diversity from an atmospheric perspective. *Current Climate Change Reports*, *5*(3), 245–257. https://doi.org/10.1007/s40641-019-00138-7

Otto-Bliesner, B. L., Brady, E. C., Fasullo, J., Jahn, A., Landrum, L., Stevenson, S., & Strand, G. (2016). Climate variability and change since 850 CE: An ensemble approach with the community Earth system model. *Bulletin of the American Meteorological Society*, *97*(5), 735–754. https://doi.org/10.1175/bams-d-14-00233.1

Paek, H., Yu, J.-Y., & Qian, C. (2017). Why were the 2015/2016 and 1997/1998 extreme El Niños different? *Geophysical Research Letters*, *44*(4), 1848–1856.

PAGES2k Consortium. (2017). A global multiproxy database for temperature reconstructions of the Common Era. *Scientific Data*, *4*.

Palmer, W. C. (1965). *Meteorological Drought* (Vol. 30). US Department of Commerce.Weather Bureau.

Parsons, L., & Hakim, G. (2019). Local regions associated with interdecadal global temperature variability in the last millennium reanalysis and CMIP5 models. *Journal of Geophysical Research: Atmospheres*, *124*(17–18), 9905–9917. https://doi.org/10.1029/2019jd030426

Parsons, L. A., Amrhein, D. E., Sanchez, S. C., Tardif, R., Brennan, M. K., & Hakim, G. J. (2021). Do multi-model Ensembles improve reconstruction skill in paleoclimate data assimilation? *Earth and Space Science*, *8*(4), e2020EA001467. https://doi.org/10.1029/2020ea001467

Patricola, C. M., O'Brien, J. P., Risser, M. D., Rhoades, A. M., O'Brien, T. A., Ullrich, P. A., & Collins, W. D. (2020). Maximizing ENSO as a source of western US hydroclimate predictability. *Climate Dynamics*, *54*(1–2), 351–372. https://doi.org/10.1007/s00382-019-05004-8

Perkins, W. A., & Hakim, G. (2020). Linear inverse modeling for coupled atmosphere-ocean ensemble climate prediction. *Journal of Advances in Modeling Earth Systems*, *12*(1), e2019MS001778. https://doi.org/10.1029/2019ms001778

Perry, S., McGregor, S., Gupta, A. S., England, M., & Maher, N. (2020). Projected late 21st century changes to the regional impacts of the El Niño-Southern Oscillation. *Climate Dynamics*, *54*(1), 395–412. https://doi.org/10.1007/s00382-019-05006-6

Rayner, N., Parker, D. E., Horton, E., Folland, C. K., Alexander, L. V., Rowell, D., & Kaplan, A. (2003). Global analyses of sea surface temperature, sea ice, and night marine air temperature since the late nineteenth century. *Journal of Geophysical Research: Atmospheres*, *108*(D14). https://doi.org/10.1029/2002jd002670

Ren, H.-L., & Jin, F.-F. (2011). Niño indices for two types of ENSO. *Geophysical Research Letters*, *38*(4). https://doi.org/10.1029/2010gl046031

Rustic, G. T., Koutavas, A., Marchitto, T. M., & Linsley, B. K. (2015). Dynamical excitation of the tropical pacific ocean and ENSO variability by little ice age cooling. *Science*, *350*(6267), 1537–1541. https://doi.org/10.1126/science.aac9937

Sanchez, S. C., Hakim, G. J., & Saenger, C. P. (2021). Climate model teleconnection patterns govern the Niño-3.4 response to early Nineteenth-century volcanism in coral-based data assimilation reconstructions. *Journal of Climate*, *34*(5), 1863–1880. https://doi.org/10.1175/jcli-d-20-0549.1

Seager, R., & Hoerling, M. (2014). Atmosphere and ocean origins of North American droughts. *Journal of Climate*, *27*(12), 4581–4606. https://doi.org/10.1175/jcli-d-13-00329.1

Sheffield, J., Goteti, G., & Wood, E. F. (2006). Development of a 50-year high-resolution global dataset of meteorological forcings for land surface modeling. *Journal of Climate*, *19*(13), 3088–3111. https://doi.org/10.1175/jcli3790.1

Sheffield, J., Wood, E. F., & Roderick, M. L. (2012). Little change in global drought over the past 60 years. *Nature*, *491*(7424), 435–438. https://doi.org/10.1038/nature11575

Shin, S.-I., Sardeshmukh, P. D., & Webb, R. S. (2010). Optimal tropical sea surface temperature forcing of North American drought. *Journal of Climate*, *23*(14), 3907–3917. https://doi.org/10.1175/2010jcli3360.1

Siler, N., Kosaka, Y., Xie, S.-P., & Li, X. (2017). Tropical ocean contributions to California's surprisingly dry El Niño of 2015/16. *Journal of Climate*, *30*(24), 10067–10079. https://doi.org/10.1175/jcli-d-17-0177.1

Steiger, N. J., Smerdon, J. E., Cook, E. R., & Cook, B. I. (2018). A reconstruction of global hydroclimate and dynamical variables over the Common Era. *Scientific Data*, *5*, 180086. https://doi.org/10.1038/sdata.2018.86

Sterl, A., van Oldenborgh, G. J., Hazeleger, W., & Burgers, G. (2007). On the robustness of ENSO teleconnections. *Climate Dynamics*, *29*(5), 469–485. https://doi.org/10.1007/s00382-007-0251-z

Stevenson, S. (2012). Significant changes to ENSO strength and impacts in the twenty-first century: Results from CMIP5. *Geophysical Research Letters*, *39*(17). https://doi.org/10.1029/2012gl052759

Stevenson, S., Fasullo, J. T., Otto-Bliesner, B. L., Tomas, R. A., & Gao, C. (2017). Role of eruption season in reconciling model and proxy responses to tropical volcanism. *Proceedings of the National Academy of Sciences*, *114*(8), 1822–1826. https://doi.org/10.1073/pnas.1612505114

Stevenson, S., Fox-Kemper, B., Jochum, M., Neale, R., Deser, C., & Meehl, G. (2012). Will there be a significant change to El Niño in the twenty-first century? *Journal of Climate*, *25*(6), 2129–2145. https://doi.org/10.1175/jcli-d-11-00252.1

Stevenson, S., Otto-Bliesner, B., Fasullo, J., & Brady, E. (2016). El Niño like" hydroclimate responses to last millennium volcanic eruptions. *Journal of Climate*, *29*(8), 2907–2921. https://doi.org/10.1175/jcli-d-15-0239.1

Stevenson, S., Overpeck, J. T., Fasullo, J., Coats, S., Parsons, L., Otto-Bliesner, B., & Cole, J. (2018). Climate variability, volcanic forcing, and last millennium hydroclimate extremes. *Journal of Climate*, *31*(11), 4309–4327. https://doi.org/10.1175/jcli-d-17-0407.1

Stevenson, S., Timmermann, A., Chikamoto, Y., Langford, S., & DiNezio, P. (2015). Stochastically generated north american megadroughts. *Journal of Climate*, *28*(5), 1865–1880. https://doi.org/10.1175/jcli-d-13-00689.1

Takahashi, K., Montecinos, A., Goubanova, K., & Dewitte, B. (2011). ENSO regimes: Reinterpreting the canonical and Modoki El Niño. *Geophysical Research Letters*, *38*(10). https://doi.org/10.1029/2011gl047364

Tardif, R., Hakim, G. J., Perkins, W. A., Horlick, K. A., Erb, M. P., Emile-Geay, J., & Noone, D. (2019). Last Millennium Reanalysis with an expanded proxy database and seasonal proxy modeling. *Climate of the Past*, *15*(4). https://doi.org/10.5194/cp-15-1251-2019

Tejedor, E., Steiger, N., Smerdon, J., Serrano-Notivoli, R., & Vuille, M. (2021b). Global temperature responses to large tropical volcanic eruptions in paleo data assimilation products and climate model simulations over the Last Millennium. *Paleoceanography and Paleoclimatology*, *36*(4), e2020PA004128. https://doi.org/10.1029/2020pa004128

Tejedor, E., Steiger, N. J., Smerdon, J. E., Serrano-Notivoli, R., & Vuille, M. (2021a). Global hydroclimatic response to tropical volcanic eruptions over the last millennium. *Proceedings of the National Academy of Sciences*, *118*(12). https://doi.org/10.1073/pnas.2019145118

Timmermann, A., An, S.-I., Kug, J.-S., Jin, F.-F., Cai, W., & Capotondi, A. (2018). othersEl Niño-southern oscillation complexity. *Nature*, *559*(7715), 535–545. https://doi.org/10.1038/s41586-018-0252-6

Ting, M., & Hoerling, M. P. (1993). Dynamics of stationary wave anomalies during the 1986/87 El Niño. *Climate Dynamics*, *9*(3), 147–164. https://doi.org/10.1007/bf00209751

Trenberth, K. E. (1997). The definition of El niño. *Bulletin of the American Meteorological Society*, *78*(12), 2771–2778. https://doi.org/10.1175/1520-0477(1997)078<2771:tdoeno>2.0.co;2

Trenberth, K. E., & Stepaniak, D. P. (2001). Indices of el Niño evolution. *Journal of Climate*, *14*(8), 1697–1701. https://doi.org/10.1175/1520-0442(2001)014<1697:lioeno>2.0.co;2

Weng, H., Ashok, K., Behera, S. K., Rao, S. A., & Yamagata, T. (2007). Impacts of recent El Niño Modoki on dry/wet conditions in the Pacific rim during boreal summer. *Climate Dynamics*, *29*(2–3), 113–129. https://doi.org/10.1007/s00382-007-0234-0

Weng, H., Behera, S. K., & Yamagata, T. (2009). Anomalous winter climate conditions in the pacific rim during recent El Niño Modoki and El Niño events. *Climate Dynamics*, *32*(5), 663–674. https://doi.org/10.1007/s00382-008-0394-6

Williams, I. N., & Patricola, C. M. (2018). Diversity of ENSO events unified by convective threshold sea surface temperature: A nonlinear ENSO index. *Geophysical Research Letters*, *45*(17), 9236–9244. https://doi.org/10.1029/2018gl079203

Xie, S.-P. (2020). Ocean warming pattern effect on global and regional climate change. *AGU Advances*, *1*(1), e2019AV000130. https://doi.org/10.1029/2019av000130

Yeh, S.-W., Kirtman, B. P., Kug, J.-S., Park, W., & Latif, M. (2011). Natural variability of the central Pacific El Niño event on multi-centennial timescales. *Geophysical Research Letters*, *38*(2). https://doi.org/10.1029/2010gl045886

Yeh, S.-W., Kug, J.-S., Dewitte, B., Kwon, M.-H., Kirtman, B. P., & Jin, F.-F. (2009). El Niño in a changing climate. *Nature*, *461*(7263), 511. https://doi.org/10.1038/nature08316

Yu, J.-Y., Zou, Y., Kim, S. T., & Lee, T. (2012). The changing impact of El Niño on US winter temperatures. *Geophysical Research Letters*, *39*(15). https://doi.org/10.1029/2012gl052483

Zhang, W., Wang, L., Xiang, B., Qi, L., & He, J. (2015). Impacts of two types of La Niña on the NAO during boreal winter. *Climate Dynamics*, *44*(5–6), 1351–1366. https://doi.org/10.1007/s00382-014-2155-z

Zhou, Z.-Q., Xie, S.-P., Zheng, X.-T., Liu, Q., & Wang, H. (2014). Global warming-induced changes in El Niño teleconnections over the North pacific and North America. *Journal of Climate*, *27*(24), 9050–9064. https://doi.org/10.1175/jcli-d-14-00254.1

Zhu, F., Emile-Geay, J., Hakim, G. J., King, J., & Anchukaitis, K. J. (2020). Resolving the differences in the simulated and reconstructed temperature response to volcanism. *Geophysical Research Letters*, *47*(8), e2019GL086908. https://doi.org/10.1029/2019gl086908